FINAL REPORT

DOE award # DE-SC0006539

Prediction of Thermal Transport Properties of Materials with Microstructural Complexity

PI: Youping Chen, University of Florida

TABLE OF CONTENTS

1. Executive summary

This project aims at overcoming the major obstacle standing in the way of progress in dynamic multiscale simulation, which is the lack of a concurrent atomistic-continuum method that allows phonons, heat and defects to pass through the atomistic-continuum interface. The research has led to the development of a concurrent atomistic-continuum (CAC) methodology for multiscale simulations of materials microstructural, mechanical and thermal transport behavior. Its efficacy has been tested and demonstrated through simulations of dislocation dynamics and phonon transport coupled with microstructural evolution in a variety of materials and through providing visual evidences of the nature of phonon transport, such as showing the propagation of heat pulses in single and polycrystalline solids is partially ballistic and partially diffusive. In addition to providing understanding on phonon scattering with phase interface and with grain boundaries, the research has contributed a multiscale simulation tool for understanding of the behavior of complex materials and has demonstrated the capability of the tool in simulating the dynamic, *in situ* experimental studies of nonequilibrium transient transport processes in material samples that are at length scales typically inaccessible by atomistically resolved methods.

2. A comparison of the actual accomplishments with the goals and objectives of the project

Goals and objectives of the project

The two goals of this project are:

(a) Establishing a concurrently coupled atomistic-continuum methodology,
(b) Demonstrating the methodology through simulation and predictions of microstructural, mechanical and thermal transport properties of thermoelectric materials.

The following objectives are proposed towards the goals:

(1) Reformulate the classical statistical mechanical theory of transport processes to unify atomistic and continuum descriptions of balance laws
(2) Recast the governing equations to facilitate coarse-scale finite element simulation of discontinuous material behavior
(3) Establish a concurrent atomistic-continuum simulation tool to simultaneously study microstructural, mechanical, and phonon transport properties of sub-millimeter sized materials
(4) Verify the formulation and simulation tool through fully atomistic simulations
(5) Validate through comparing simulation results of popular thermoelectric materials with experimental measurements
(6) Predict the lowest possible phonon thermal conductivity in SrTiO3 ceramics

Actual Accomplishments: [1-31]

In addressing **Goal (a) and Objective (1)**, we have examined and analyzed existing formalisms for linking molecular and continuum descriptions of transport processes and properties. We have used analytical and simulation results to show that the widely used atomistic formulas for momentum and heat fluxes are not applicable to transient transport processes or highly inhomogeneous systems, e.g., materials with atomically sharp interfaces. We have identified the origin of this problem and formulated a new method for formally deriving microscopic conservation equations and expressions for momentum and heat fluxes. The formulation builds on the nonequilibrium statistical mechanical theory of Kirkwood, but differing from the Irving and Kirkwood formalism that uses the differential form of conservation equations, the new formalism derives the integral representation of conservation laws. The formulation then naturally leads to the expressions of fluxes as a measure of the flow of a physical property through a surface per unit area per unit time. The resulting flux formulas are mathematically rigorous, fully

consistent with the physical concepts of momentum and heat fluxes, and applicable to nonequilibrium transient processes in atomically inhomogeneous systems with general many-body forces. The results of this work are documented and published in two journal papers.

In addressing **Goal (a) and Objective (2) and (3)**, we have recast the balance equations in terms of internal force density, atomic-scale displacements, and kinetic temperature, thereby lifting the requirement of displacement continuity and allowing simulations of defects, including dislocations and cracks, to emerge as a consequence of the governing equations without special numerical treatment. The numerical implementation of the formulation naturally leads to the concurrent atomistic-continuum (CAC) method that can pass waves, heat, and defects from the atomic to the continuum regions and can serve as a space and time resolved simulation tool for simulation of simultaneously microstructural, mechanical and phonon thermal transport behavior.

In addressing **Goal (b) and Objective (4)**, we have verified the CAC method through comparing CAC results with molecular dynamics (MD) simulation results. The current version of the code has been tested through simulations of dislocation nucleation and multiplication, and through propagations of monochromatic waves and heat pulses that excite all allowable phonons of the materials. We have simulated a variety of materials, including Cu, Al, Si, SrTiO3, LiF, Bi2Te3, PbTe single and polycrystals, Si-Ge superlattices, and have compared the accuracy and efficiency with respect to MD simulation. These comparisons have demonstrated that, with significantly less degrees of freedom than that in MD, CAC can reproduce microstructural, mechanical, and phonon thermal transport behavior and properties in good agreement with MD.

In addressing **Goal (b) and Objective (5)**, we have compared CAC simulation results with existing experimental measurements and observations, including dislocation structure, grain boundary structures, fracture failure patterns, thermal conductivity, phonon drag coefficients, and phonon focusing patterns. The comparisons show that CAC can reproduce the atomic details of grain boundary structures of SrTiO3, microscale dislocation structures in Si, and also the six fold phonon focusing pattern in single crystal Si.

In addressing **Goal (b) and Objective (6),** we have modelled and simulated $SrTiO_3$ single crystal, bicrystals, polycrystals with general grain boundaries and with twin boundaries. CAC simulations of polycrystalline $SrTiO_3$ have reproduced the microstructural evolution as a result of the interactions between dislocations and between dislocations and grain boundaries under mechanical loading, including the nucleation and propagation of dislocations. The stress-strain responses, the velocity of dislocations and the distances they travel are also measured.

We have also simulated $SrTiO_3$ single crystal and polycrystals under thermal loading, measured the thermal conductivity and plotted the thermal conductivity as a function of twin spacing, which reveals a minimum thermal conductivity at a critical twin spacing. We then attempted to construct a hierarchically structured $SrTiO_3$ that contains twining boundaries within each gran in a polycrystals, and predicted the lowest thermal conductivity.

In addressing **Goal (b),** we have developed a phonon representation of ultrafast laser pulse using the Bose-Einstein phonon frequency distribution for the simulation of pump-probe experiments. The development of the heat pulse model allows simulation and visualization of a variety of phenomena, including phonon focusing, wave interference, dislocation drag, interfacial Kapitza resistance caused by quasi-ballistic phonon transport, etc. Most importantly, visualization of the space and time-resolved materials responses enable us to clearly identify the nature of phonon transport, the mechanisms for phonon scattering by coherent or semi-coherent phase interfaces, by grain boundary interfaces, and by both stationary and mobile dislocations.

3. A Summary of Project Activities

3.1 Nonequilibrium statistical mechanics formulation of transport equations and properties for highly transient transport processes and inhomogeneous materials

We have examined existing formalisms for linking molecular and continuum governing equations and for deriving microscopic formulas for momentum and heat fluxes. We have used both analytical and simulation results to show that the widely used flux formulas are not applicable to transient transport processes or inhomogeneous systems, e.g., superlattices and metamaterials. A new formalism is developed for deriving microscopic momentum and heat fluxes. The resulting flux formulas are shown to satisfy both differential and integral forms of conservation laws, in addition to being consistent with the physical meaning of fluxes. Simulations of the propagation of heat pulses in superlattices and metamaterials confirm that the formulas are applicable to nonequilibrium transient processes in atomically inhomogeneous systems with general many-body forces[6, 7].

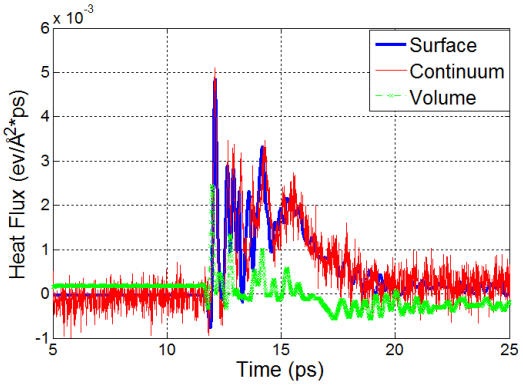

FIG. 1 Energy flux measured at an interface of a superlattice under pulsed heating averaged over two symmetric planes. Each data point is averaged over 100 time steps. The pulse inputs a total of 100 eV over 10 fs to the center region of the model. *Surface* denotes the new *surface-averaged heat flux formula; Volume*: the volume-averaged heat flux formula, which is the most popular heat flux formula in the literature and implemented in LAMMPS; *Continuum*: the energy flux obtained from the Continuity Equation through measuring the change of the total energy in a region to obtain the flow of energy across the surface enclosing the region. The overlap of the heat flux by the *Surface* and *Continuum* formulas indicates the validity of the new formula for local heat flux.

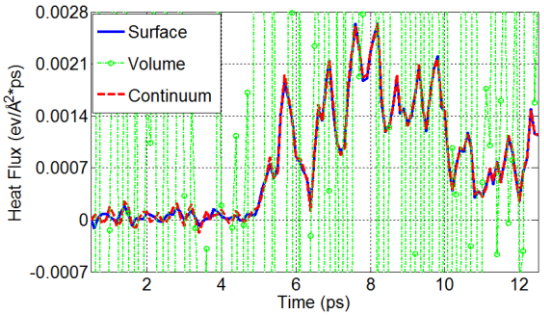

FIG. 2 Energy flux measured at an interface of a Si phononic crystal (with periodical holes) under pulsed heating averaged over two symmetric planes. Each data point is averaged over 100 time steps. The pulse inputs a total of 100 eV over 10 fs to the center region of the model. Note that the spurious fluctuations in heat flux using the popular volume formula are more profound for the Si phononic crystal.

3.2 CAC code development

(1) CAC Fortran and C^{++} codes

For a concurrent atomistic-continuum formulation, existing numerical methods developed for continuum or particle methods need to be modified or reformulated. New methods that have been developed for CAC include (1) a new discretization scheme for a two-level material description, (2) a recast form of the governing equations to remove inter-element connectivity requirements, (3) special finite element shapes to admit the full complement of cleavage or slip planes, (4) special type of element to model regions with defects such as grain boundaries in polyatomic materials; (5) adaptive mesh refinement techniques for simulation of dynamic evolution of defects, and (6) lattice dynamics-based shape functions to address short wavelength phenomena in the coarse-scale finite element domain**.** The current versions of CAC codes are written in FORTRAN and C++, respectively.

(2) Passing waves of all wavelengths from the atomic to the continuum region

Spurious wave reflection at the interfaces of concurrent multiscale method is a well-known challenge. With a single set of governing equations for both the atomistic and continuum descriptions, CAC reduces this problem to a numerical problem with non-uniform mesh, which is a long-standing problem in the finite element method whose non-uniform mesh causes wave reflection at the interfaces of different numerical resolutions, as shown in FIG. 3

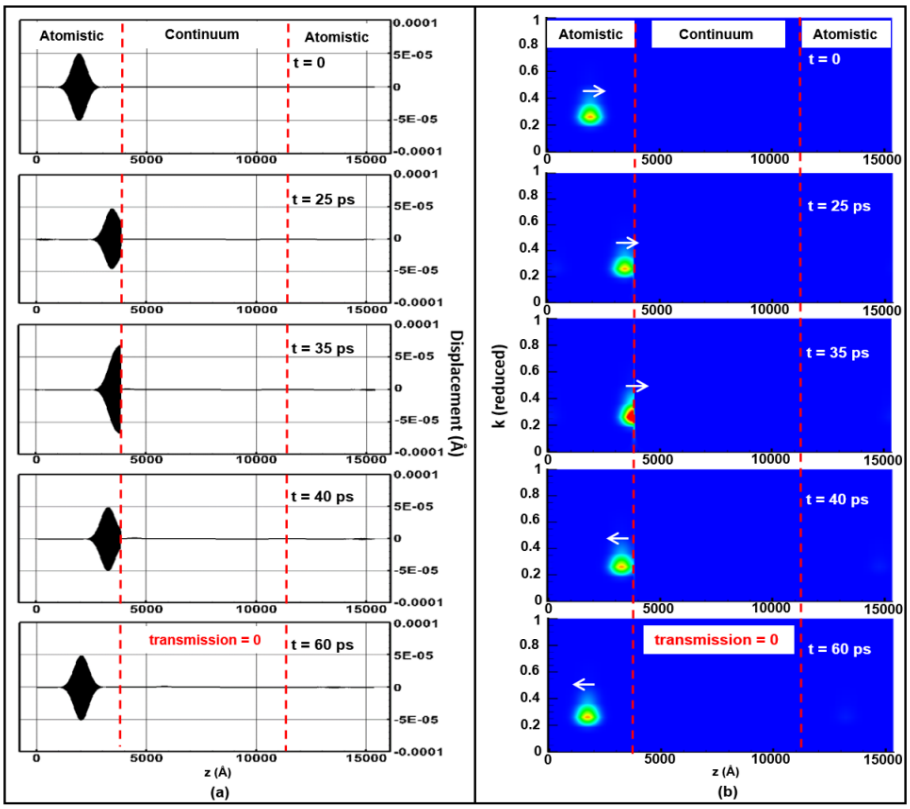

FIG. 3 Wave-packet ($k_o = 0.25$) reflection by the atomic-continuum interface in a CAC simulation with linear shape functions; (left) the time sequence of the spatial distribution of the displacement, and (right) the time sequence of the spatial distribution of the wavevector k from a wavelet analysis.

To address this problem, we have formulated and implemented a lattice dynamics formulation of finite element shape functions to enable a full phonon representation in the continuum description of a CAC model. This then permits the passage of short-wavelength phonon waves from the atomistic to continuum regions. The benchmark examples showing in FIG.4 demonstrate that the new shape functions enable the passage of all allowable phonons through the atomistic-continuum interface; it also preserves the wave coherency and energy conservation after phonons transport across multiple atomistic-continuum interfaces. The work is the first step towards developing a concurrent atomistic-continuum simulation tool for non-equilibrium phonon-mediated thermal transport in materials with microstructural complexity [33].

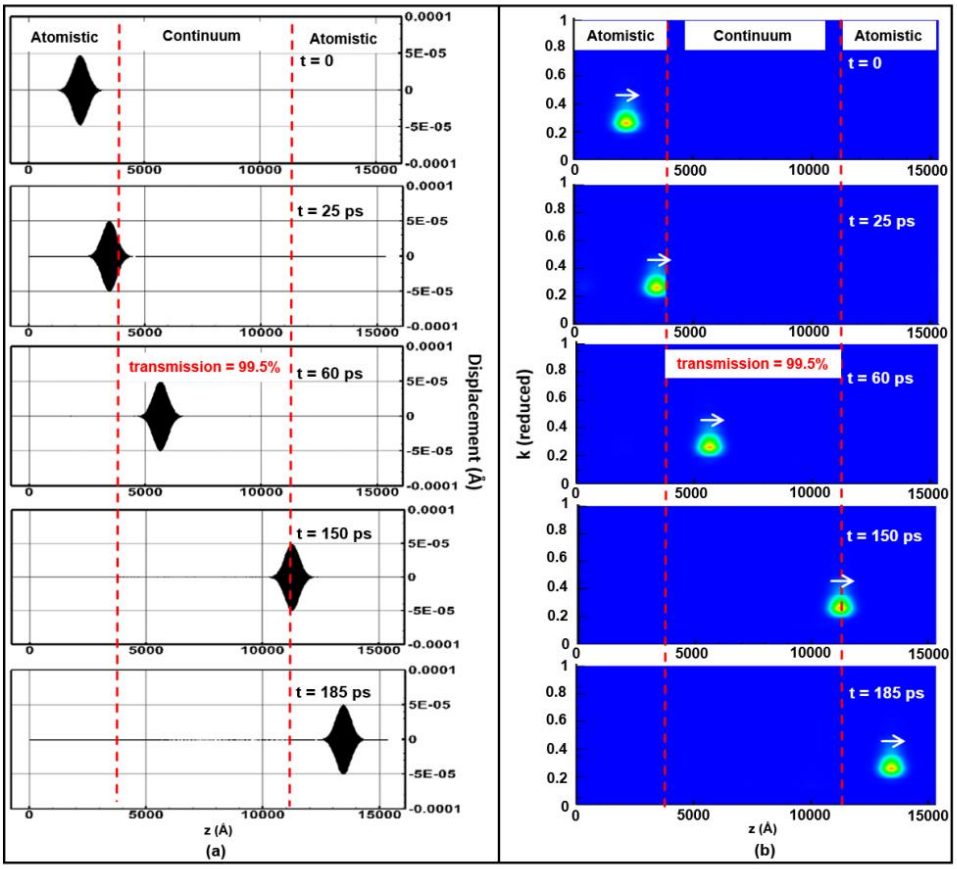

FIG. 4 Wave-packet ($k_o = 0.25$) transmission across the atomic-continuum interface in a CAC simulation with the new FE shape functions; left: time sequence of spatial distribution of the displacement; right: time sequence of the spatial distribution of the wavevector k from a wavelet analysis.

For phonons whose wavelengths are longer than a critical wave length determined by the size of the element, CAC can precisely predict the phonon dynamics and phonon transport. To verify that there is no spurious wave reflection at the atomistic-continuum interface for long wavelength phonons, a single crystal model is discretized with both uniform mesh and non-uniform mesh, i.e., with both coarse mesh and atomistically-resolved fine mesh. A CAC simulation is then conducted along with the phonon heat pulse model, which continuously generate phonons with wavelengths ranging from 5nm to 250nm. The heat source is applied to the center of the models where the coarse elements are employed. The simulation not only demonstrate the smooth passage of phonons across the numerical interfaces, but also has captured the remarkable phenomenon of phonon focusing, which is the tendency for the ballistic heat flux emitted from a point source to concentrate along certain directions of the crystal, as shown in FIG. 5 [1].

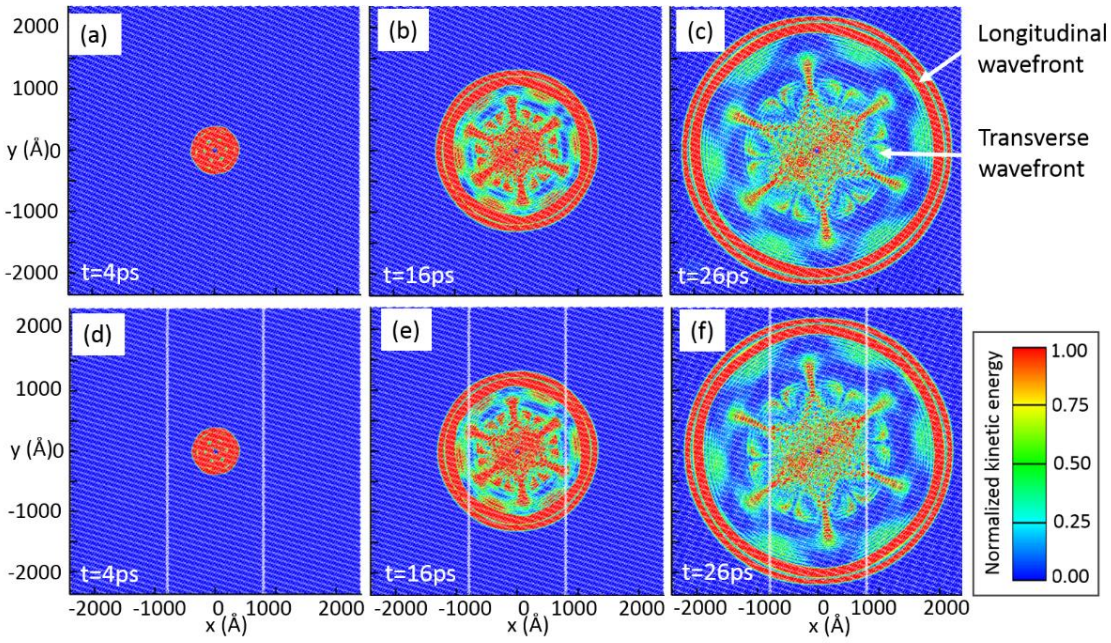

FIG. 5 Comparison of the phonon wave propagation in the single crystal specimen constructed with a uniform coarse mesh (a-c) and a non-uniform mesh that has both atoms and coarse-scale finite elements (d-f). Note that the phenomenon of phonon focusing is reproduced in the simulations

(3) Passing defects from the atomic to the continuum region

We have also tested and demonstrated that CAC allows the smooth passage of dislocations through sharp interfaces between the atomic and the coarse-scale finite element domains without aphysical reflection of dislocations or the need for heuristic rules to pass the dislocations. Complex dislocation phenomena such as dislocation nucleation, dynamic strain bursts associated with nucleation and migration avalanches, formations of Lomer-Cottrell locks, dislocation boundary interactions, formation of intrinsic and extrinsic stacking faults, deformation twinning, and curved dislocation loops all have been reproduced by the CAC method, cf. FIG. 6. CAC simulation results were also shown to compare well with MD simulation results [29].

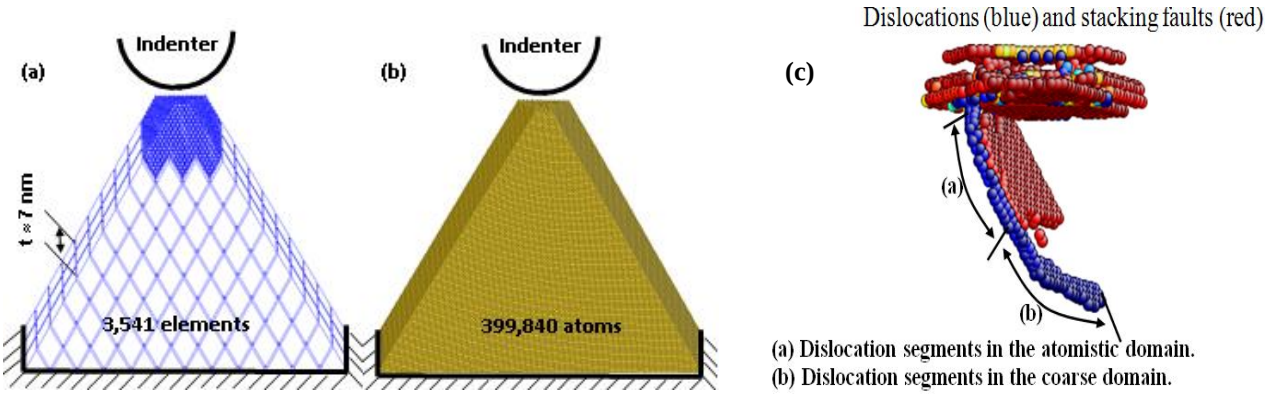

FIG. 6 (a) A CAC model (with 3541 elements) and (b) a MD model (with 399,840 atoms) under indentation; (c) curved dislocations (blue) and stacking faults (red) propagated from the atomic to the continuum regions without reflection.

3.3 Verification of the CAC method by comparing CAC with MD simulation results

(1) Reproducing MD simulation results of wave propagation

Different from existing popular mesoscale simulation methods, CAC is a space and time-resolved simulation methods that can reproduce dynamic phenomena. To verify CAC in reproducing MD simulation results of wave propagation, we have simulated the propagation of continuous monochromatic radial waves and compare the simulation results with MD, as shown in FIG. 7 [34].

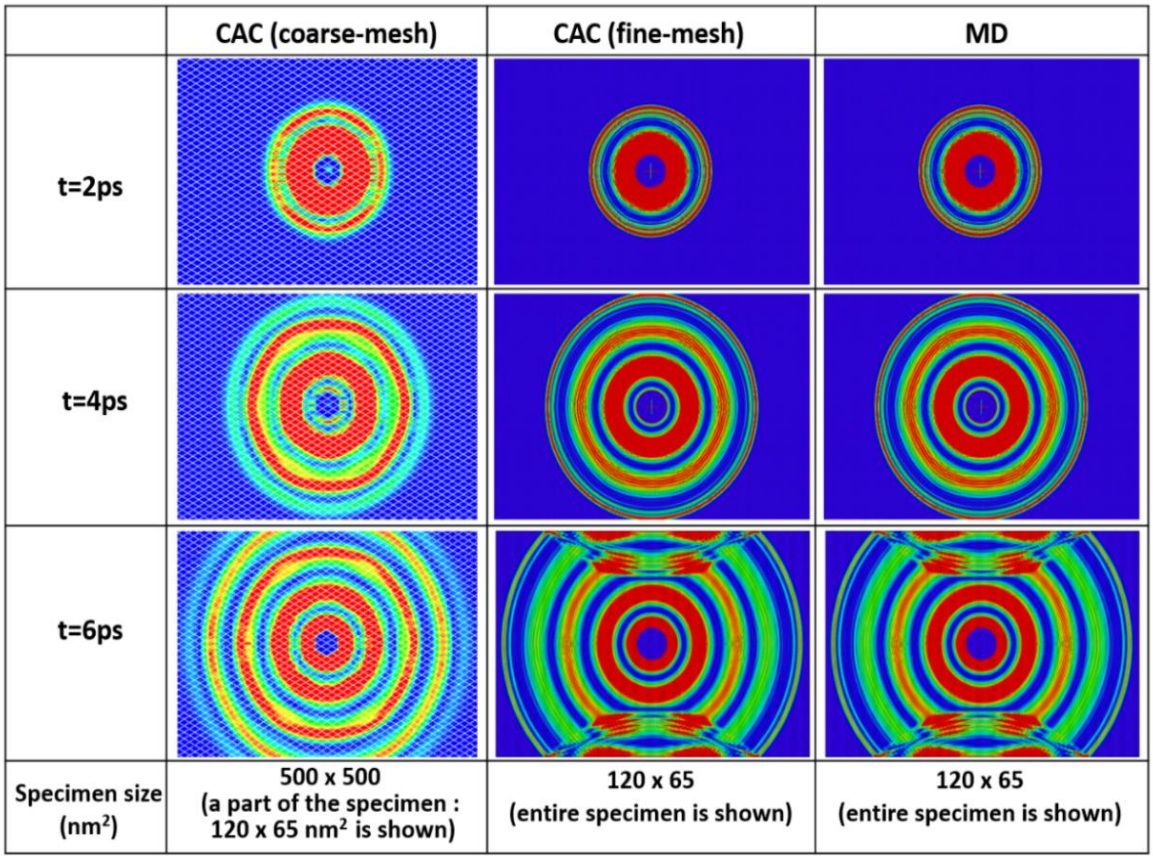

FIG. 7 Comparison of simulation results of a monochromatic wave propagation in CAC and in MD.

As can be seen from FIG.7, when the mesh size approaches the atomic resolution, the CAC simulation with fine mesh generates the same results as MD. Note that the limited specimen size induces wave reflections by the surface. With coarse-graining, a larger computer model is simulated, and the exploded view of the same region around the heat source is presented in the first column for comparison. It is seen that the phonon wavelength, group velocity, and the wave crests in slight hexagonal shape caused by phonon focusing are reproduced by CAC with a coarse mesh in agreement with MD results.

(2) Reproducing MD simulation results of dislocation loop growth

Submicron-sized samples with 42,000 finite elements containing up to ~86 million atoms have been simulated using a concurrent atomistic-continuum method. The simulations not only reproduce nucleation and growth of semicircular dislocation loops in Cu and Al from voids, but also hexagonal shuffle dislocation loops in Si, with loop radius approaching ~75nm. Meanwhile, details of leading and trailing partial dislocations connected by intrinsic stacking faults, dislocation loop coalescence through annihilation, and formation of junctions are reproduced. One comparison between CAC and MD simulation results is shown in FIG. 8 [32].

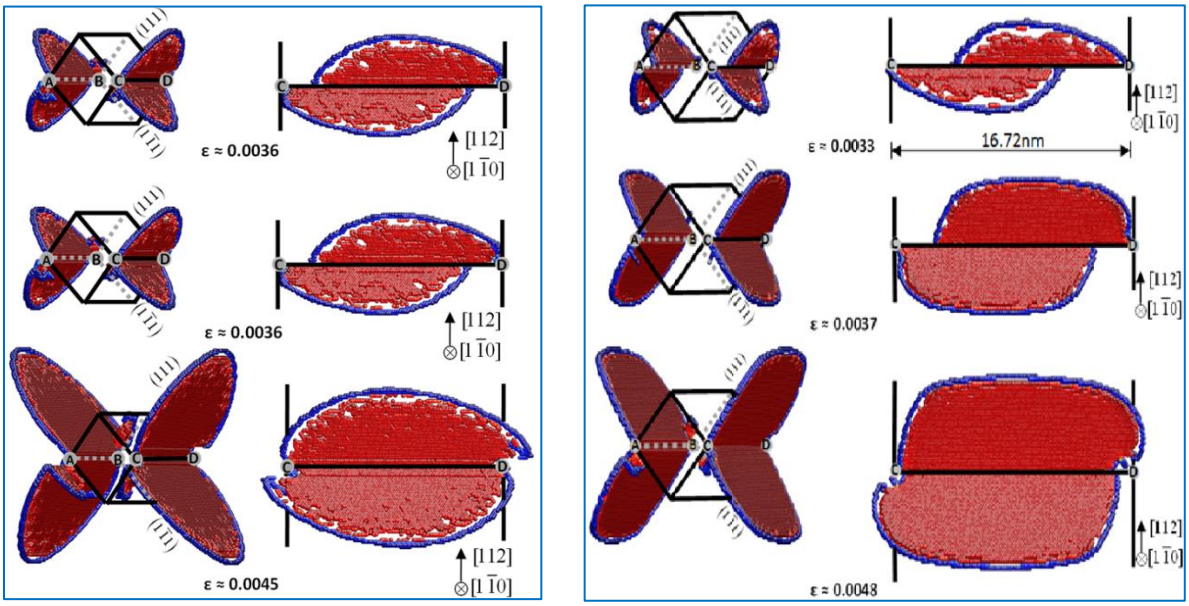

FIG. 8 Comparison of strain sequences of dislocations (blue) and stacking faults (red) comparing dislocation loop simulated by CAC results (left) and by MD simulation results (right), showing very good agreement between CAC and MD simulation results.

(3) Reproducing MD simulation results of fast moving dislocations

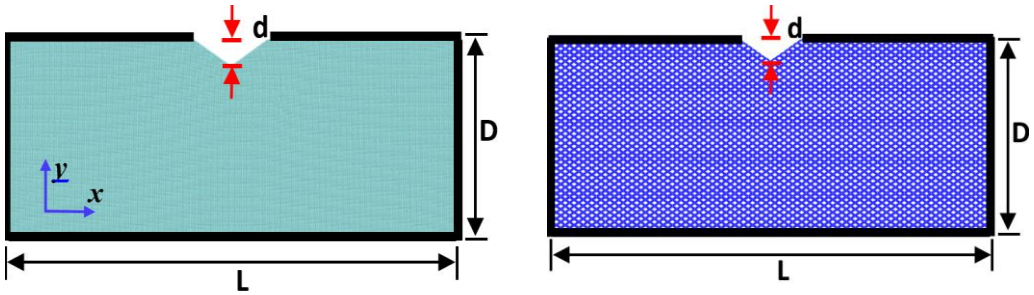

FIG. 9 Atomistic model of 4 million atoms and CAC model with 40K elements for simulation of dislocation nucleation and fast propagation.

Direct experimental observation of sonic dislocations in solids was not possible until an alternative material, a plasma crystal, was recently developed. Given that the inter-particle distance in plasma crystals is on the order of 100 μm or above, characteristic frequencies are on the order of 100 Hz or below, and the speed of sound in a plasma crystal is on the order of 10 mm/s, experiments on plasma crystals can provide qualitative understanding of dynamic behavior of sonic dislocations in certain solids. However, such experiments cannot provide precise information regarding the velocity, acoustic phonon emission, or core stress fields of fast moving dislocations in crystalline metals. The CAC method is shown to be able to reproduce the dynamics of fast moving dislocation in good agreement with MD [10].

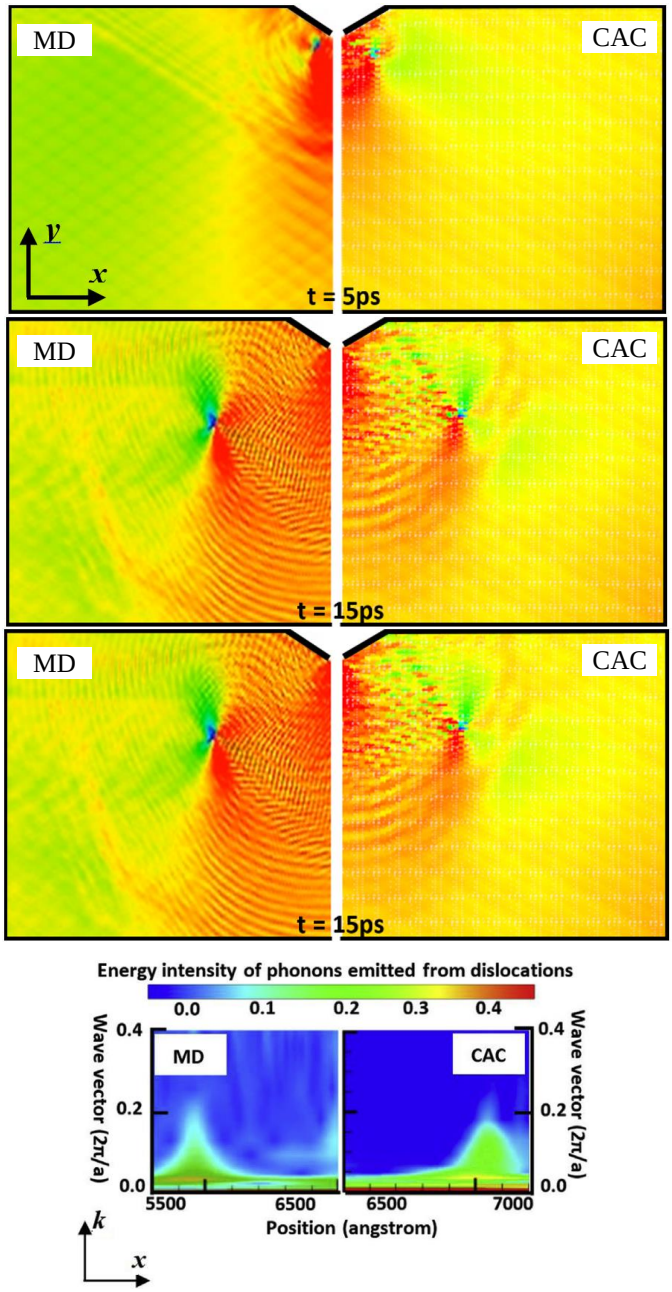

FIG. 10 Time sequences of dislocation motions using MD and coarse-grained (CG) simulations using CAC showing the dislocation speed and phonon emitted by the moving dislocation.

(4) Reproducing MD simulation results of dislocation-grain boundary interaction and microstructural evolution in SrTiO3

For SrTiO3 polycrystals, we have compared CAC and MD simulation results of a same computer model. The results show that (1) as long as the atomic region of the GB region is sufficiently large, CAC can reproduce the exact displacement and strain field near the GB region, as shown in FIG.11, and (2) dislocation nucleation from grain boundaries and the subsequent propagation into grains, as shown in FIG. 12. [14, 18, 19]

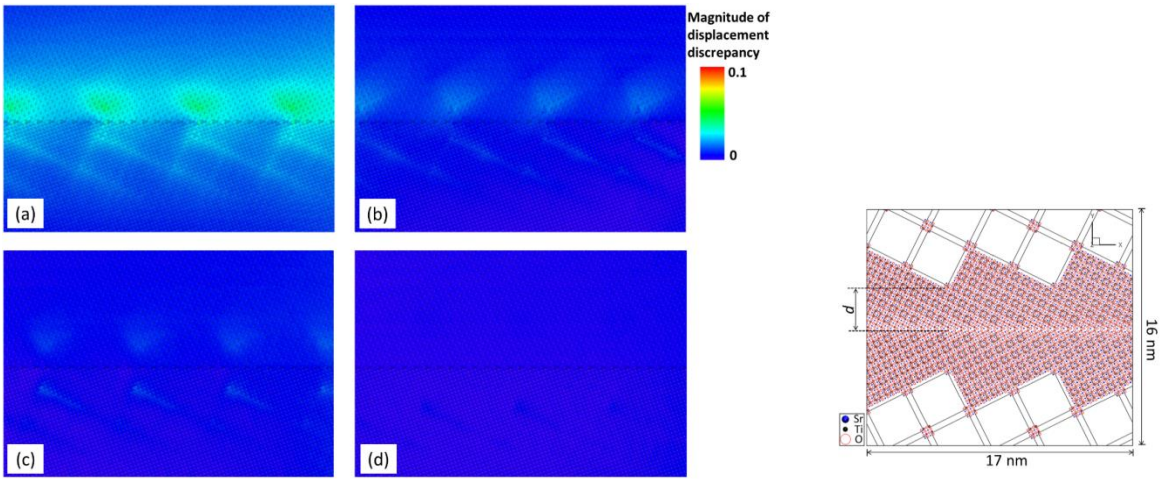

FIG. 11. The magnitude of atomic-level displacement discrepancy between CAC and MD simulation results of the ∑5 (210) model with different *d* (the smallest distance between the atomic-continuum interface and the GB): (a). 7.0Å; (b). 8.73Å; (c). 12.22Å; (d). 26.2Å.

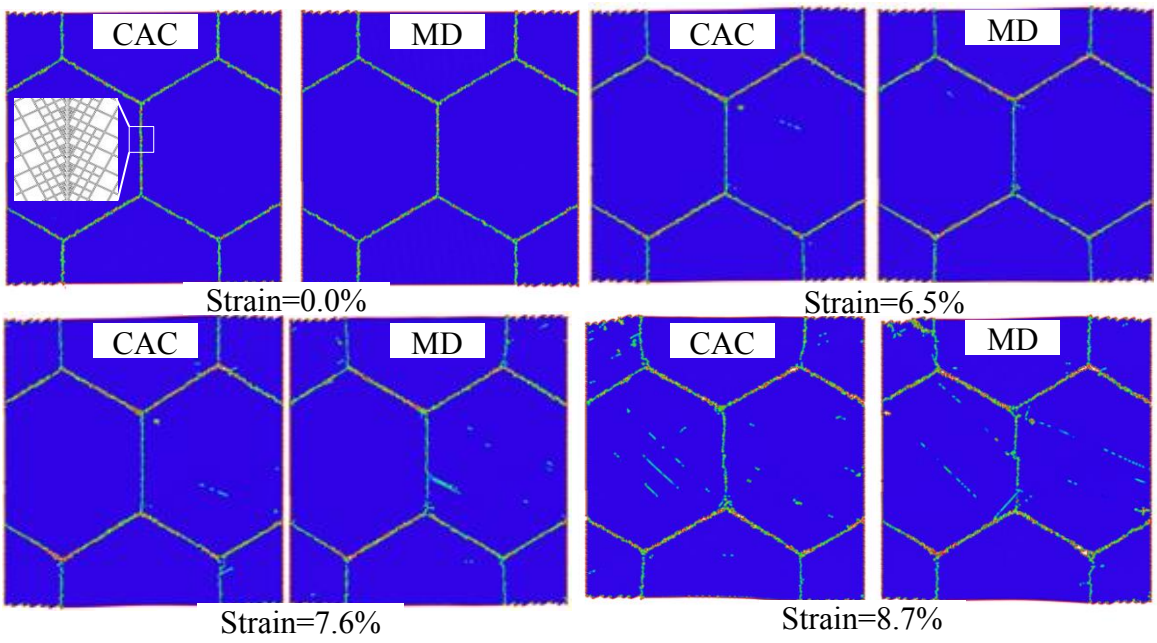

FIG.12 . Contour plots of the center symmetry parameter in CAC and MD simulations of SrTiO3 polycrystals under compression showing dislocation nucleation and interaction with grain boundaries in good agreement between CAC and MD results of such complex responses.

3.4 Validation of CAC through comparing CAC simulations with experimental measurements

(1) Reproduce the grain Boundary Structures in $SrTiO_3$

To simulate mechanical and thermal transport properties of materials with microstructure, we need to reproduce the microstructure of the materials. The equilibrium grain boundary (GB) structures in $SrTiO_3$ tilt ∑5 (210) GB with initial translation state of (0.0 0.5 1.5) have been obtained by DFT calculations and also by experimental techniques including High Angular Annular Dark Field Scanning Transmission Electron Microscopy (HAADF-STEM) by Lee et al. (PRB, 83, 2011), in which the main objective was to find the stable GB structures in $SrTiO_3$.

To test the CAC method in reproducing microstructural properties, we have also simulated $SrTiO_3$ with tilt grain boundaries. A comparison between CAC and DFT results of the outlined unit structure around the GB plane shows that these results from CAC are in excellent agreement with those obtained by DFT, including both the shape of the GB structural units and the arrangement of ions within the units. Moreover, CAC simulation has also reproduced the concomitant misalignment of the ions within the (Ti, O) columns, i.e., the O ions are further inwards (towards the boundary plane) than the Ti ions after relaxation, in exact correspondence with the DFT calculation. The GB unit structure composed of Sr and Ti ions obtained by CAC also compares well with that by HAADF-STEM experimental image obtained by Lee et al, as shown in FIG. 13 [18].

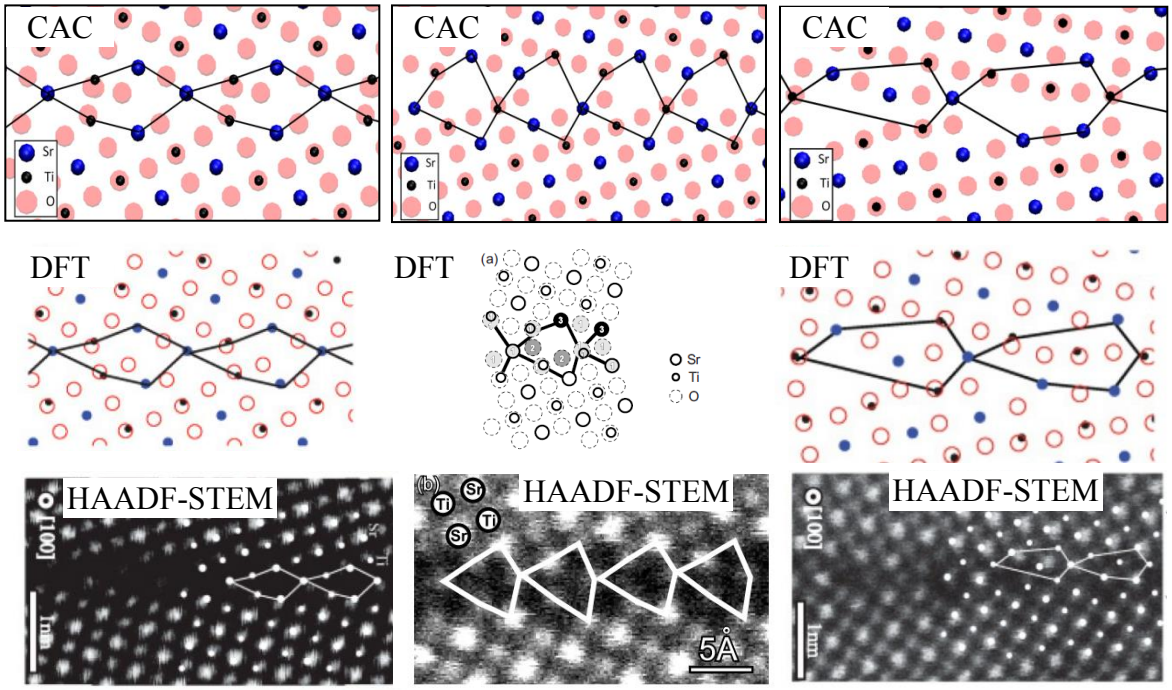

FIG. 13 CAC simulation results of the local GB structure (left) ∑5(210) translation (0.0, 0.5, 1.5) , (middle) GB structures of ∑5(310) translation (4.5, 0.5, 0.5), and (right) GB structures of ∑13(510) translation (5.0, 1.0, 0.0), compared with density functional theory (DFT) result from Lee et al. (the second row) (PRB, 83, 2011) , and HAADF-STEM results (the third row) (PRB, 83, 2011), showing a very good agreement between CAC, DFT and experimental measurement results.

(2) Reproduce the structure and shape of dislocation loops in Silicon

The nucleation and growth of dislocation loops have been investigated by extensive experimental studies in the past half century. It has been observed that dislocation loops nucleate at the atomic scale and evolve into large scale loops with radii of 30~100 nm or larger. The hexagonal shape of shuffle dislocation loops in Si has been experimentally observed, as shown in FIG 14 (left). We have simulated the nucleation of dislocation loops from voids and the growth into large loops in Si. Our simulation results have reproduced the experimentally observed hexagonal shape of dislocation loops in Si, cf. FIG. 14[31].

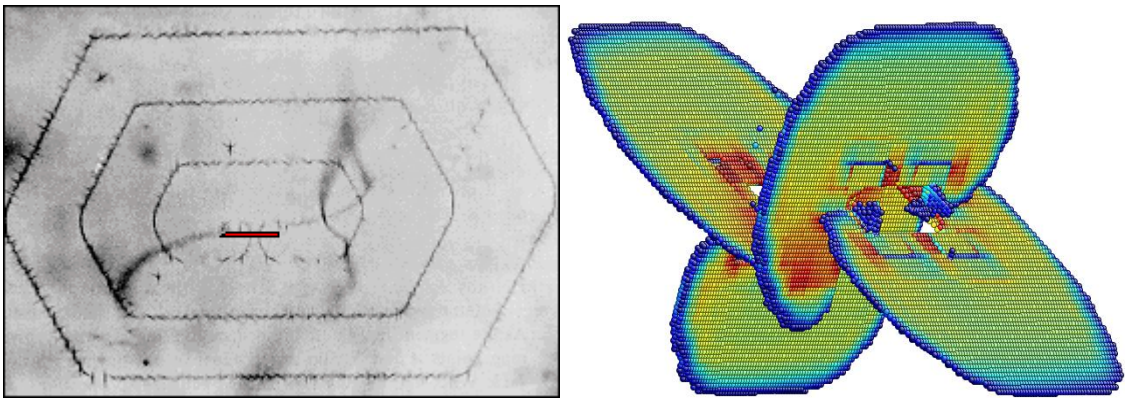

FIG. 14 Left: a 2D image of dislocation loops in Si; the dislocation loops show the symmetry of the {111} slip plane (Barrett, Nix, and Tetelman, The Principles of Engineering Materials, Prentice Hall 1973); Right: 3D view of CAC simulation results of dislocation loops in Si. The comparison shows a good agreement between CAC and experimental observation of dislocation loops in Si.

(3) Dislocation Depinning from Voids

Experimental studies indicate that voids act as obstacles to dislocations, and, when by passed, lead to localization of deformation. To test CAC in reproducing such phenomena, we simulated dislocation-void interaction and compared with existing experimental observation. The three-stage dislocation-obstacle interaction process is captured by CAC: (1) dislocation line encountered the obstacles; (2) dislocation line was pinned by the surfaces of obstacles; and (3) dislocation line broke away from the obstacles in materials under a critical shear stress, in good agreement with experimental observations [16].

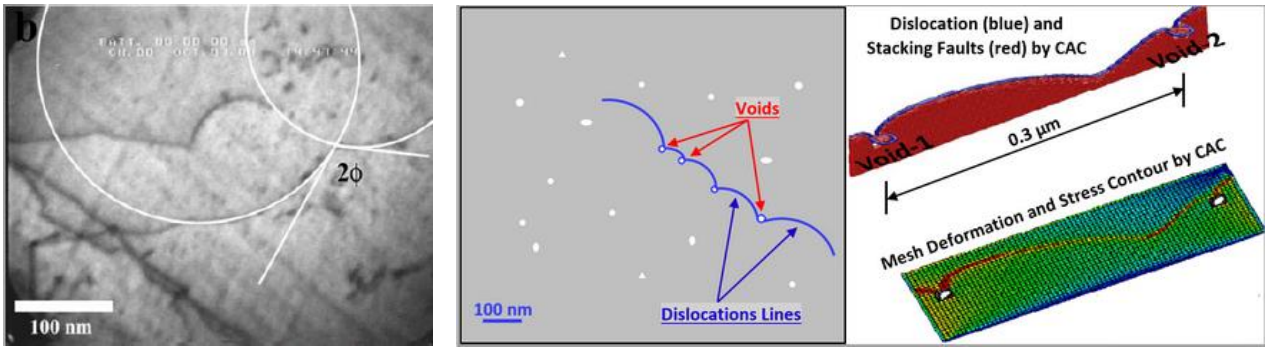

FIG. 15. Comparison of experimental images of dislocation depinings from voids by Gary in 2007 and CAC simulations results; left and middle: experimental results; right CAC simulation results.

(4) Reproducing the phonon focusing pattern in Si

A variety of caustics are observed in the phonon images of crystals. These "*caustics*" are intense concentrations of heat flux. They are the result of phonon focusing. Phonon focusing is the tendency for the ballistic heat flux emitted from a point source to concentrate along certain directions of the crystal. The formation of phonon focusing caustics is a transient process. The phenomenon was explained by James P. Wolf that the intense concentration of heat flux occurs "because the number of phonons emitted from the heat source along one crystalline direction differs from that emitted along another". The phonon focusing pattern observed in Si has been reported to have a six-fold symmetry by Wichard and Dietsche in 1992 and by Kolomenskii and Maznev in 1993. CAC has reproduced this phenomenon and the formation process in the simulation of heat pulse propagation in Si, as shown in FIG. 16.

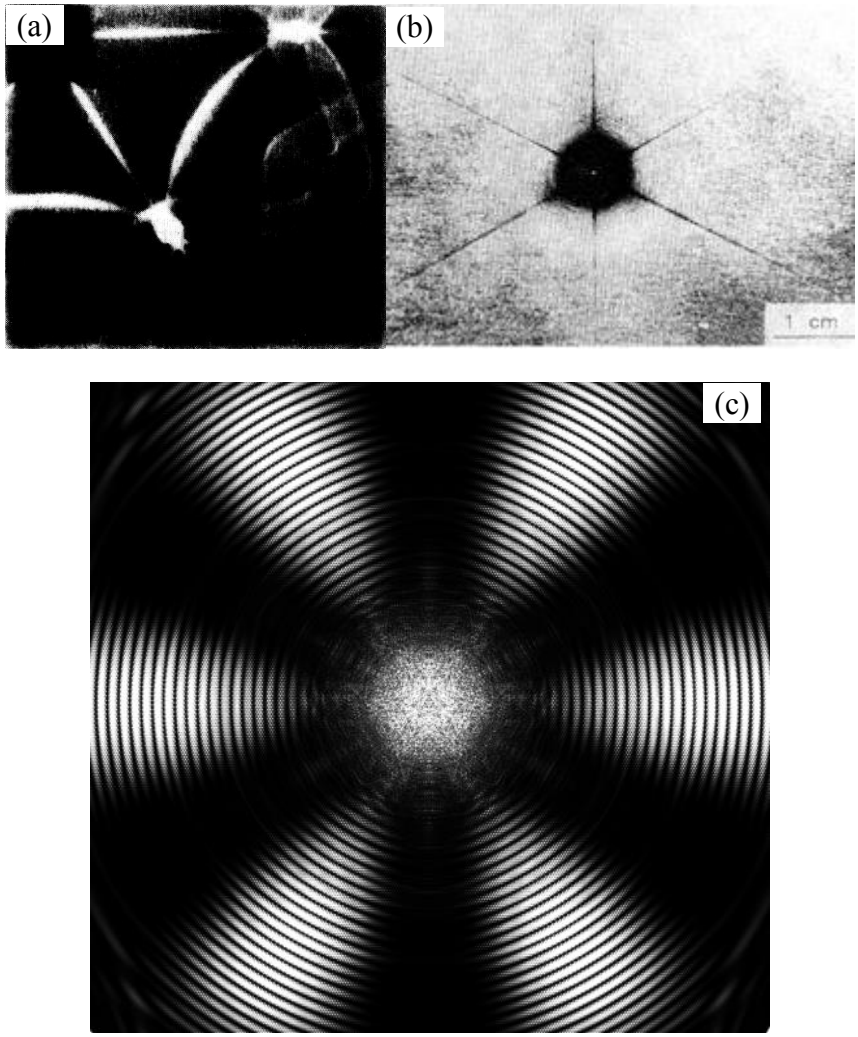

FIG.16 Phonon focusing caustics observed (a) by Wichard and Dietsche in 1992 (*PRB,* 48**,** 14502), (b) by Kolomenskii and Maznev in 1993 (PRB, 45**,** 9705), and (c) by CAC simulation of heat pulse propagation in Si single crystal kinetic; the snapshot was taken as the kinetic energy contour projected on (111) crystal plane; the Si single crystal model is constructed with uniform finite elements. The model contains 360K elements, for the specimen of 460 million atoms.

3.5 **CAC simulations of SrTiO3 polycrystals**

We have performed atomistic and CAC simulation of $SrTiO_3$ polycrystals with various grain size. These simulations demonstrate CAC in simultaneously reproducing the microstructural, mechanical and thermal transport behavior of polyatomic materials, and in measuring mechanical and thermal transport properties.

(1) Microstructural evolution and dislocation nucleation, propagation, and interaction with GBs

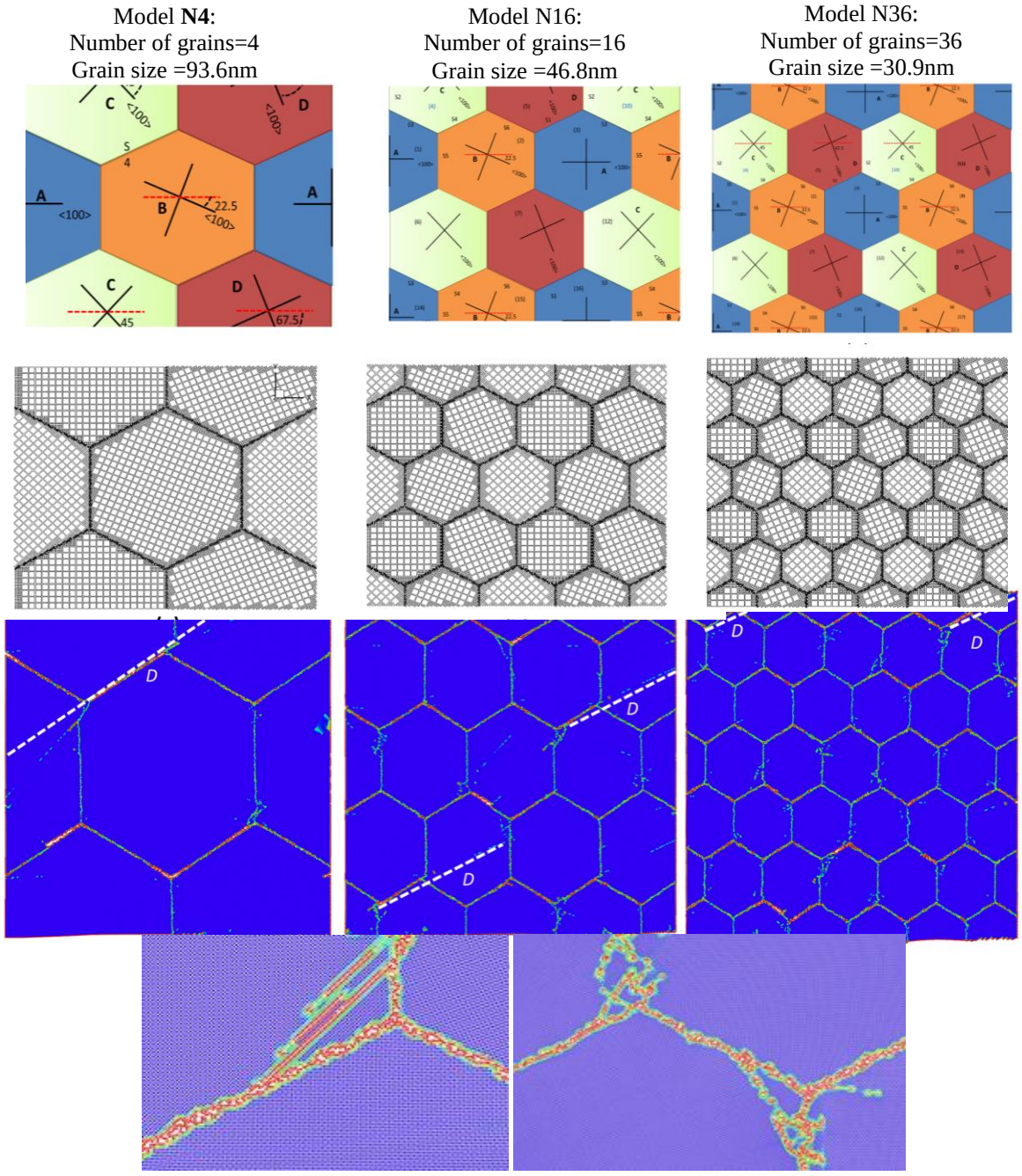

FIG. 17 CAC simulation results of SrTiO3 polycrystals under compression, row 1-3: the computer models; row 4: simulation results which show dislocation nucleation, propagation and interaction with GBs; the maximum dislocation travel distance: $D^{\mathrm{Max}}_{(\mathrm{N4})} > D^{\mathrm{Max}}_{(\mathrm{N16})} > D^{\mathrm{Max}}_{(\mathrm{N36})}$; row 4: snapshots of the deformation at triple junctions [20].

(2) Phonon thermal transport through tilt grain boundaries in SrTiO3

We have also performed wave-packet simulations to obtain phonon mode-dependent energy transmission coefficients across Σ5 grain boundaries in SrTiO3. We then use the Landauer formalism to calculate thermal conductivity and compare the results with direct measurements of thermal conductivity in steady-state simulations. The results show that the Landauer formalism can yield thermal conductivity consistent with that directly measured in steady-state simulations, as shown in FIG. 18 [22].

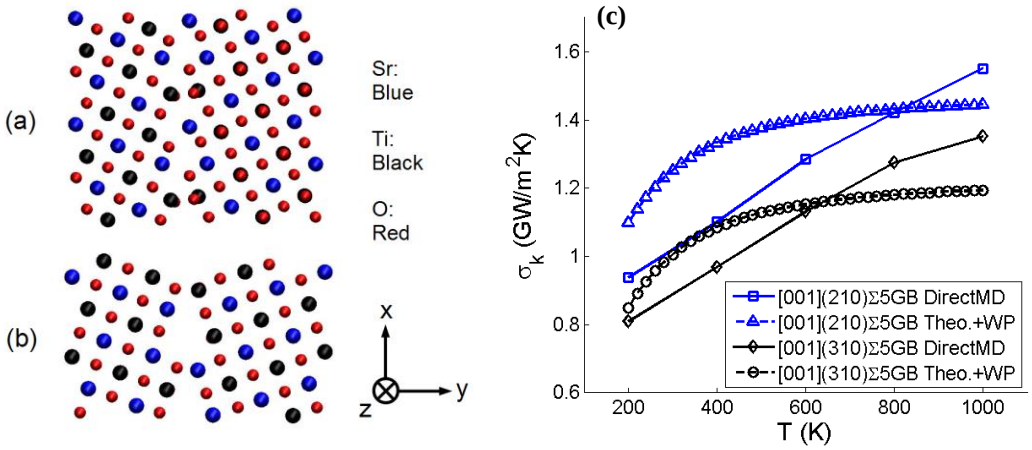

FIG. 18. The GB structure of (a) [001] (210) Σ5 and (b) [001] (310) Σ5. Temperature dependence of the Kapitza conductance measured through steady-state simulation and calculated theoretically using Landauer formalism with transmission coefficients determined from transient simulation of wave packets.

(3) Minimum thermal conductivity in $SrTiO_3$ with periodical twin boundaries

To investigate the thermal conductivity in $SrTiO_3$, we have simulated periodically twinned $SrTIO_3$. Simulation results suggest that the thermal conductivity of $SrTiO_3$ can be significantly reduced through incorporating twin boundaries; the thermal conductivity of nano-twinned STO can be reduced by $60-70$ %, compared to that of single crystal $SrTiO_3$; Simulation results also show that periodically twinned $SrTiO_3$ exhibits a minimum in thermal conductivity at a critical twin spacing, and the critical twin spacing is found to increase with the size of the specimen. In addition, the results of the effect of simulation cell size reveal an appreciable contribution from long wavelength phonons to the thermal conductivity of twinned $SrTiO_3$, as shown in FIF. 20 [11].

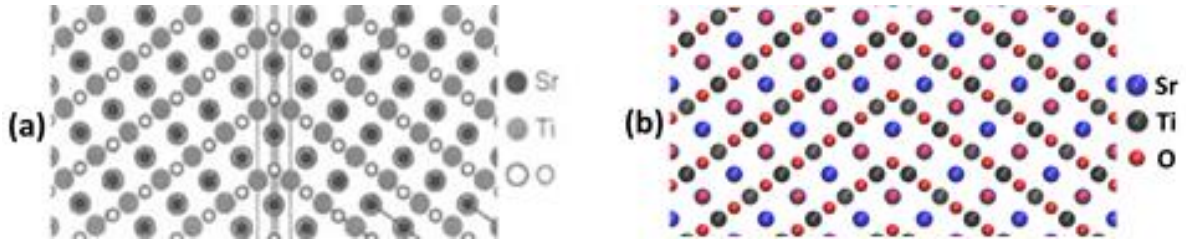

FIG. 19 The Σ3 SrTiO3 twin boundary structure observed by HRTEM (Kienzle *et al.)*; (b)The Σ3 SrTiO3 twin boundary structure obtained in the simulation.

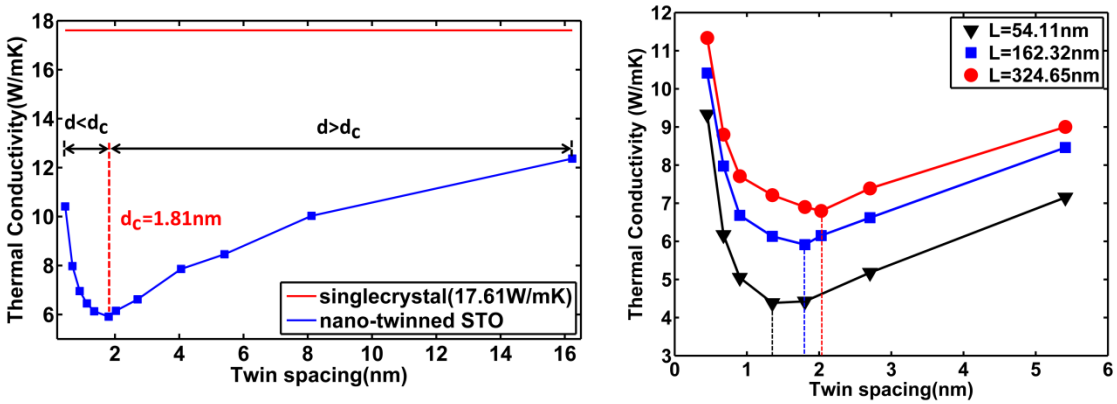

FIG. 20. Cross-plane thermal conductivity of nano-twinned STO with specimen size of 162.32nm. Thermal conductivity of twinned STO with different specimen length.

If the periodical twin boundaries can be introduced in the grains of a polycrystalline $SrTiO_3$, as shown in FIG. 21, the thermal conductivity can be further reduced. The lowest thermal conductivity at room temperature is predicted to be ~1.9 – 3.0 W/mK.

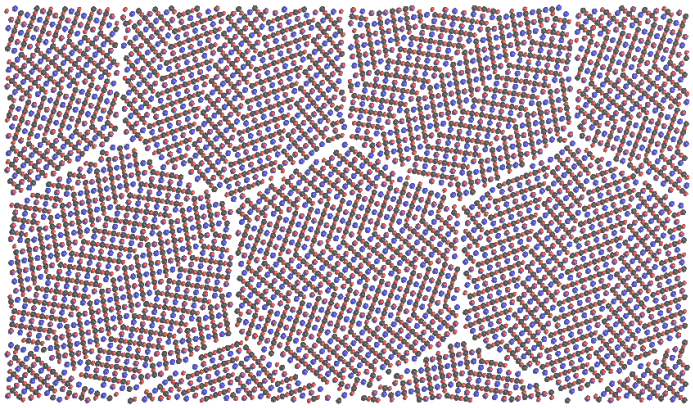

FIG. 21. A hierarchical structural model of a $SrTiO_3$ polycrystalline sample with periodical twin boundaries within each grain.

3.6 CAC simulation of phonon interaction with dislocations, phase interfaces and grain boundaries

Experimental studies of phonon transport using direct photoexcitation have led to observations of many new phenomena. One observation that is of principal significance is the non-diffusive heat propagation in non-metallic crystals, especially those with interfaces. The ballistic-diffusive phonon transport and its interaction with interfaces can be manipulated to control thermal conductivity of materials, which can lead to significant scientific and technological advances. The need for a better understanding of phonon transport has in turn driven the development of experimental techniques such as the time domain thermo-reflectance (TDTR) and related ultrafast pump-probe techniques that utilize ultrafast laser pulses.

To simulate ultrafast pump-probe experiments, we have developed a phonon representation of ultrafast laser pulses. Since the CAC method is a coarse-grained method derived bottom up from the atomistics, and can adapt the viewpoint of phonons to describe heat and temperature in terms of mechanical vibrations, the phonon representation of heat pulse model naturally fits in the framework of CAC.

(1) Ballistic-diffusive phonon transport in single and polycrystals

CAC heat pulse simulation results provide visual evidence that the propagation of a heat pulse in crystalline solids with or without grain boundaries is partially ballistic and partially diffusive, i.e., there is a co-existence of ballistic and diffusive phonon transport, with the long-wavelength phonons traveling ballistically while the short-wavelength phonons scatter with each other and travel diffusively. To gain a quantitative understanding of GB thermal resistance, the kinetic energy transmitted across GBs is monitored on the fly and the time-dependent energy transmission for each specimen is measured. Simulation results reveal that the energy transmission coefficient across GB is wavelength dependent and the presence of GBs modifies the nature of thermal transport, with the coherent long-wavelength phonons dominating the heat conduction in materials with GBs. In addition, it is found that the phonon-GB interaction can result in a reconstruction of GBs [1].

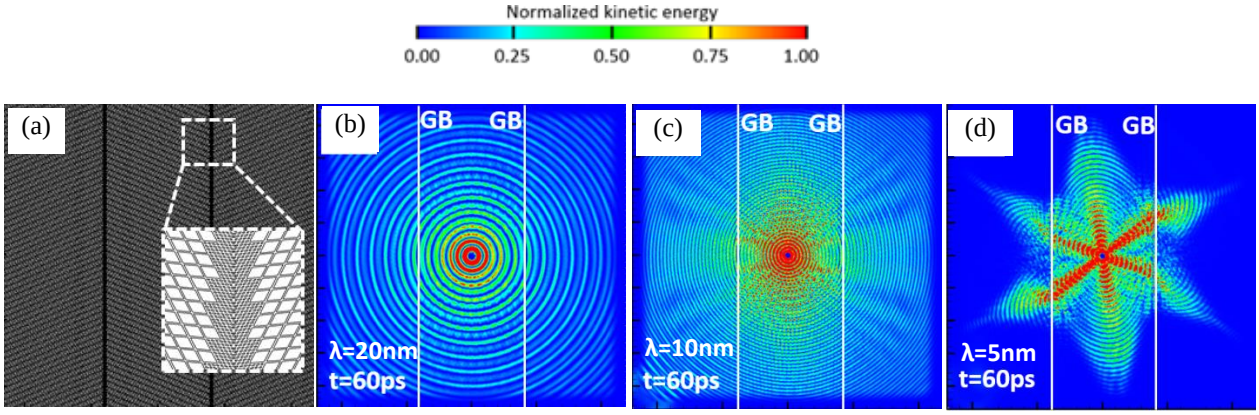

FIG. 22 (a) a computer model with two ∑19 grain boundaries (GBs); (b-d) snapshots of kinetic energy distribution during the propagation of monochromatic waves across the ∑19 GBs to demonstrate the wavelength (λ)-dependent phonon scattering and energy transmission: (b) λ=20nm, ballistic transport with 100% energy transmission; (c) λ=10nm, dominant ballistic transport with partially spectral scattering by the GBs and 95% energy transmission; (d) λ=5nm, dominant coherent scattering by the GBs and ~50% energy transmission. Note that in (d) the formation of phonon-focusing caustics are clearly visible; these caustics change their directions after crossing the GBs.

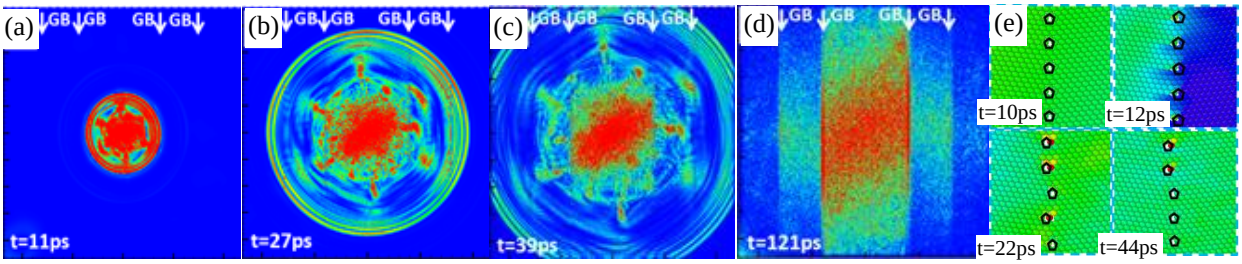

FIG.23. Snapshots of kinetic energy distribution during the propagation a heat pulse with Bose-Einstein phonon distribution (both acoustic and optical phonons) across GBs (GB locations are indicated by white arrows), showing (a-c) a simultaneous ballistic-diffuse transport and a co-existence of coherent-incoherent phonon scattering by the GBs, (a-b) phonon focusing caustics, (d) Kaptiza (GB thermal) resistance[1], and (e) zoomed-in snapshots showing the GB structural change during the heat pulse propagation.

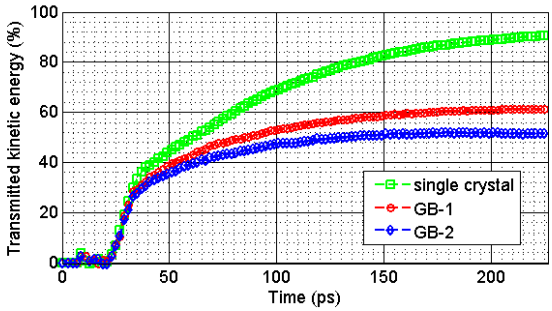

FIG.24 Time history of the accumulated percentage of transmitted kinetic energy.

(2) Phonon transport across phase boundaries in superlattices

We have also attempted to simulate phonon interaction with mobile dislocations and with interface misfit dislocations. FIGs 25-28 present CAC simulation results of phonon-phase interface and phonon-dislocation interactions to demonstrate the capability of CAC in simulation and visualization of the dynamic processes of phonon scattering. All phenomena and underlying mechanisms of phonon transport, whether coherent or diffusive, are visualized. This facilitates understanding of phonon scattering mechanisms.

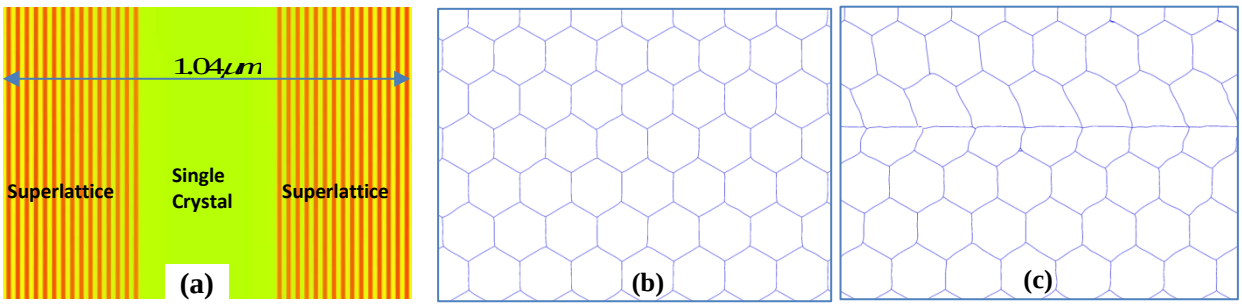

FIG. 25 (a) A CAC computer model of superlattices, (b) Misfit dislocations in a Si(111)/Ge interface obtained in a CAC simulation, showing hexagonal dislocation networks; and (c) change of the interfacial structure (the dislocation network) after a dislocation glide across the interface; blue lines in (b) and (c) represent ½[110] dislocations, obtained using dislocation extraction algorithm (DXA).

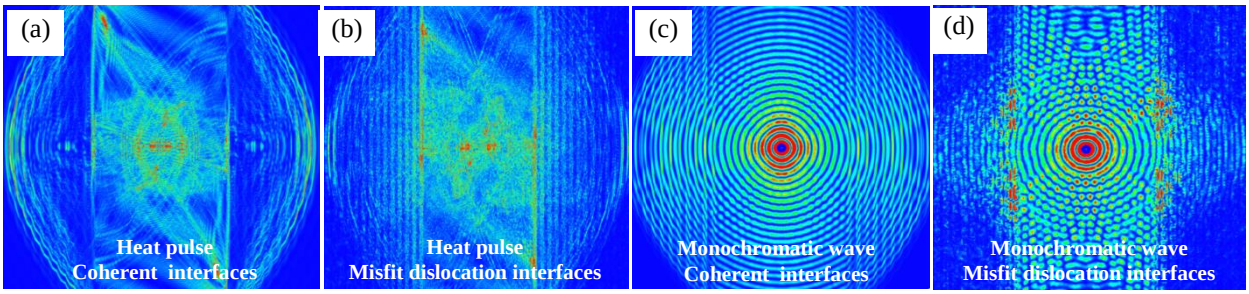

FIG. 26 Snapshots of kinetic energy distribution in a superlattice during the propagations of a heat pulse (a-b) with Plankian phonon distribution and (c-d) a monochromatic wave of wavelength 28nm, in which (a, c) coherent interfaces; (b, d) interfaces with misfit dislocations. These results show that misfit dislocations scatter most phonons diffusively, leading to significantly reduced energy transmissions.

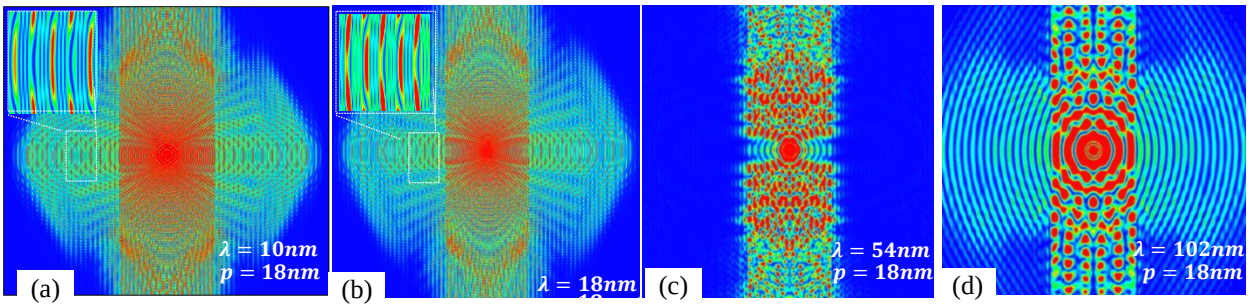

FIG. 27 Snapshots of kinetic energy distribution during the propagation of a monochromatic waves in a superlattice, as a mode-wise study of wavelength(λ)-dependent wave interference, the superlattices are composed of 60 alternating layers of two materials and the period length is p=18nm; (a) $\lambda = 10nm\ (< p)$ and (b) $\lambda = 18nm\ (= p)$, phonons partially transmit across the first interface and propagate in the superlattice with different wavelengths in the different material layers, as shown in the zoom-in figures; (c) $\lambda = 54nm\ (= 3p)$, completely reflected back, as a result of Bragg reflection; (d) $\lambda = 102nm\ (= 5p)$, ballistic transport across the superlattice with an altered wavelength of 56nm after crossing the first interface.

(3) Moving dislocations and phonon-dislocation interaction

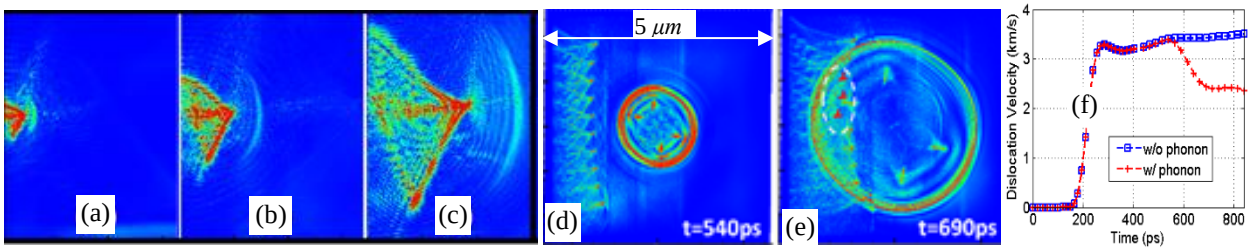

FIG. 28 (a-c) Snapshots of kinetic energy distribution during the propagation of dislocations and a heat pulse: (a-c) a moving dislocation before meeting a heat pulse, showing that the motion of the dislocation is accompanied by radial-shaped wavefronts of phonons ahead of the moving dislocation and V-shaped wave tails in the wake of the dislocation; (d-e) an array of moving dislocations meeting with a heat pulse showing partially coherent partially diffuse scattering of the phonons by the moving dislocations, and also arrest of three dislocations as a result of interaction with the heat pulse, (f) average dislocation velocity with and without propagating phonons showing that dislocations travel the distance of microns before the velocity reaches a plateau and the effect of phonons on averaged dislocation velocities [2].

4 PRODUCTS DEVELOPED UNDER THE AWARD

(a) Networks or collaborations fostered

The CAC method has attracted the attention of leading experts in the field of dislocation theory for space and time-resolved simulation of defect dynamics, leading to collaborations with Professor David McDowell from Georgia Institute of Technology. This collaboration has made CAC the first practical coarse-grained atomistic method that can serve the purposes of modeling fast moving dislocations, dislocation nucleation & multiplication, and grain boundary interactions with long-range dislocation pile-ups, with no empirical assumptions beyond interatomic potentials.

(b) Publications

The project has resulted in 2 book chapters[14, 27] and 34 journal publications (29 published[1-13, 15-26, 28-31], 2 accepted for publication [32, 33], and 3 under review).

1. Chen, X., W. Li, L. Xiong, Y. Li, S. Yang, Z. Zheng, D.L. McDowell, and Y. Chen, *Ballistic-diffusive phonon heat transport across grain boundaries.* Acta Materialia, 2017. **136**(Supplement C): p. 355-365.
2. Chen, X., L. Xiong, D.L. McDowell, and Y. Chen, *Effects of phonons on mobility of dislocations and dislocation arrays.* Scripta Materialia, 2017. **137**: p. 22-26.
3. Xu, S., L. Xiong, Y. Chen, and D.L. McDowell, *Shear stress-and line length-dependent screw dislocation cross-slip in FCC Ni.* Acta Materialia, 2017. **122**: p. 412-419.
4. Xu, S., L. Xiong, Y. Chen, and D.L. McDowell, *Comparing EAM Potentials to Model Slip Transfer of Sequential Mixed Character Dislocations Across Two Symmetric Tilt Grain Boundaries in Ni.* JOM, 2017: p. 1-8.
5. Xu, S., L. Xiong, Y. Chen, and D. McDowell, *Validation of the Concurrent Atomistic-Continuum Method on Screw Dislocation/Stacking Fault Interactions.* Crystals, 2017. **7**(5): p. 120.
6. Chen, Y. and A. Diaz, *Local momentum and heat fluxes in transient transport processes and inhomogeneous systems.* Physical Review E, 2016. **94**(5): p. 053309.
7. Chen, Y., *The origin of the distinction between microscopic formulas for stress and Cauchy stress.* EPL (Europhysics Letters), 2016. **116**(3): p. 34003.
8. Pluchino, P.A., X. Chen, M. Garcia, L. Xiong, D.L. McDowell, and Y. Chen, *Dislocation migration across coherent phase interfaces in SiGe superlattices.* Computational Materials Science, 2016. **111**: p. 1-6.
9. Xu, S., L. Xiong, Y. Chen, and D.L. McDowell, *Sequential slip transfer of mixed-character dislocations across Σ3 coherent twin boundary in FCC metals: a concurrent atomistic-continuum study.* npj Computational Materials, 2016. **2**: p. 15016.
10. Xiong, L., J. Rigelesaiyin, X. Chen, S. Xu, D.L. McDowell, and Y. Chen, *Coarse-grained elastodynamics of fast moving dislocations.* Acta Materialia, 2016. **104**: p. 143-155.
11. Li, W., X. Chen, Z. Zheng, and Y. Chen, *Minimum thermal conductivity in periodically twinned SrTiO 3.* Computational Materials Science, 2016. **112**: p. 107-112.
12. Xu, S., L. Xiong, Y. Chen, and D.L. McDowell, *Edge dislocations bowing out from a row of collinear obstacles in Al.* Scripta Materialia, 2016. **123**: p. 135-139.
13. Xu, S., L. Xiong, Y. Chen, and D.L. McDowell, *An analysis of key characteristics of the Frank-Read source process in FCC metals.* Journal of the Mechanics and Physics of Solids, 2016. **96**: p. 460-476.
14. Yang, S. and Y. Chen, *Concurrent Atomistic-Continuum Simulation of Defects in Polyatomic Ionic Materials*, in *Multiscale Materials Modeling for Nanomechanics*2016, Springer International Publishing. p. 261-296.

15. Xu, S., L. Xiong, Q. Deng, and D.L. McDowell, *Mesh refinement schemes for the concurrent atomistic-continuum method.* International Journal of Solids and Structures, 2016. **90**: p. 144-152.
16. Xiong, L., S. Xu, D.L. McDowell, and Y. Chen, *Concurrent atomistic–continuum simulations of dislocation–void interactions in fcc crystals.* International Journal of Plasticity, 2015. **65**: p. 33-42.
17. Chen, X., A. Chernatynskiy, L. Xiong, and Y. Chen, *A coherent phonon pulse model for transient phonon thermal transport.* Computer Physics Communications, 2015.
18. Yang, S. and Y. Chen, *Concurrent atomistic and continuum simulation of bi-crystal strontium titanate with tilt grain boundary.* Proceedings of the Royal Society A: Mathematical, Physical & Engineering Sciences, 2015. **471**(2175).
19. Yang, S., N. Zhang, and Y. Chen, *Concurrent atomistic–continuum simulation of polycrystalline strontium titanate.* Philosophical Magazine, 2015. **95**(24): p. 2697-2716.
20. Xiong, L., X. Chen, N. Zhang, D.L. McDowell, and Y. Chen, *Prediction of phonon properties of 1D polyatomic systems using concurrent atomistic–continuum simulation.* Archive of Applied Mechanics, 2014. **84**(9-11): p. 1665-1675.
21. Zheng, Z., X. Chen, B. Deng, A. Chernatynskiy, S. Yang, L. Xiong, and Y. Chen, *Phonon thermal transport through tilt grain boundaries in strontium titanate.* Journal of Applied Physics, 2014. **116**(7): p. 073706.
22. Xiong, L. and Y. Chen, *Predicting phonon properties of 1D polyatomic chains through the concurrent atomistic-continuum simulations.* Archive of Applied Mechanics, 2014. **84**(9-11): p. 1665-1675.
23. Chen, X., L. Xiong, A. Chernatynskiy, and Y. Chen, *A molecular dynamics study of tilt grain boundary resistance to slip and heat transfer in nanocrystalline silicon.* Journal of Applied Physics, 2014. **116**(24): p. 244309.
24. Xiong, L., D.L. McDowell, and Y. Chen, *Sub-THz Phonon drag on dislocations by coarse-grained atomistic simulations.* International Journal of Plasticity, 2014. **55**: p. 268-278.
25. Yang, S., L. Xiong, Q. Deng, and Y. Chen, *Concurrent atomistic and continuum simulation of strontium titanate.* Acta Materialia, 2013. **61**(1): p. 89-102.
26. Deng, Q. and Y. Chen, *A coarse-grained atomistic method for 3D dynamic fracture simulation.* Journal for Multiscale Computational Engineering, 2013. **11**(3): p. 227-237.
27. Xiong, L., Q. Deng, and Y. Chen, *Coarse-Grained Atomistic Simulations of Dislocation and Fracture in Metallic Materials*, in *Handbook of Micromechanics and Nanomechanics*2013, Pan Stanford Publishing.
28. Xiong, L., Q. Deng, G. Tucker, D.L. McDowell, and Y. Chen, *A concurrent scheme for passing dislocations from atomistic to continuum domains.* Acta Materialia, 2012. **60**(3): p. 899-913.
29. Xiong, L., Q. Deng, G.J. Tucker, D.L. McDowell, and Y. Chen, *Coarse-grained atomistic simulations of dislocations in Al, Ni and Cu crystals.* International Journal of Plasticity, 2012. **38**: p. 86-101.
30. Xiong, L. and Y. Chen, *Coarse-grained atomistic modeling and simulation of inelastic material behavior.* Acta Mechanica Solida Sinica, 2012. **25**(3): p. 244-261.
31. Xiong, L., D.L. McDowell, and Y. Chen, *Nucleation and growth of dislocation loops in Cu, Al and Si by a concurrent atomistic-continuum method.* Scripta Materialia, 2012. **67**(7): p. 633-636.
32. Chen, X., A. Diaz, L. Xiong, D.L. McDowell, and Y. Chen, *Passing Waves from Atomistic to Continuum.* Journal of Computational Phyiscs, accepted.
33. Chen, X., W. Li, A. Diaz, Y. Li, D.L. McDowell, and Y. Chen, Recent Progress in the Concurrent Atomistic-Continuum (CAC) Method and its Application in Phonon Transport. MRS Communications, in press.